

ARTICLE

Received 14 Jun 2013 | Accepted 5 Sep 2013 | Published 30 Sep 2013

DOI: 10.1038/ncomms3556

Demonstration of a novel focusing small-angle neutron scattering instrument equipped with axisymmetric mirrors

Dazhi Liu¹, Boris Khaykovich¹, Mikhail V. Gubarev², J. Lee Robertson³, Lowell Crow³, Brian D. Ramsey² & David E. Moncton^{1,4}

Small-angle neutron scattering (SANS) is the most significant neutron technique in terms of impact on science and engineering. However, the basic design of SANS facilities has not changed since the technique's inception about 40 years ago, as all SANS instruments, save a few, are still designed as pinhole cameras. Here we demonstrate a novel concept for a SANS instrument based on axisymmetric focusing mirrors. We build and test a small prototype, which shows a performance comparable to that of conventional large SANS facilities. By using a detector with 48- μm pixels, we build the most compact SANS instrument in the world. This work, together with the recent demonstration that such mirrors could increase the signal rate at least 50-fold, for large samples, while improving resolution, paves the way to novel SANS instruments, thus affecting a broad community of scientists and engineers.

¹Nuclear Reactor Laboratory, Massachusetts Institute of Technology, 77 Massachusetts Avenue, Cambridge, Massachusetts 02139, USA. ²Marshall Space Flight Center, NASA, VP62, Huntsville, Alabama 35812, USA. ³Instrument and Source Design Division, Oak Ridge National Laboratory, Oak Ridge, Tennessee 37831, USA. ⁴Department of Physics, Massachusetts Institute of Technology, 77 Massachusetts Avenue, Cambridge, Massachusetts 02139, USA. Correspondence and requests for materials should be addressed to B.K. (email: bkh@mit.edu).

Small-angle neutron scattering (SANS) instruments are found at nearly every neutron-research facility, where they serve a sizable and diverse community of users. The basic instrument design remains the same, as original small-angle-scattering instruments were described: a very small aperture, relative to the source size, is used to collimate the beam illuminating the sample¹. Such a design is not only very inefficient in terms of the neutron flux; it also requires complex and costly detectors, which should move inside vacuum tanks, reaching 10 m in length and more than a meter in diameter. This inefficient design is still in use after decades of developments, demonstrating the enormous challenge of building efficient optics for thermal and cold neutrons². Among notable proposals are the use of zone plates³, material and magnetic lenses^{4–6}, converging collimators⁷, multiple beams⁸ and mirrors^{9–11}. Whereas converging collimators and multiple beams are incremental improvements of the basic design, the use of focusing devices, such as lenses and mirrors, results in qualitatively different instruments, reminiscent of optical microscopes, promising to achieve higher resolution and signal rates. However, focusing devices are used very infrequently because neutron lenses and zone plates have strong chromatic aberrations and focal lengths approaching 100 m, whereas existing focusing mirrors could not collect a large enough portion of the neutron beam's phase space.

To address this challenge, we pioneered the use of axisymmetric focusing mirrors, called Wolter mirrors, which have the role of achromatic lenses with a short focal length and high throughput^{12,13}. Our ray-tracing analysis of Wolter optics showed the possibility of improving the signal rate by a factor of ≥ 50 when optimized for an existing SANS facility¹⁰. This is a very significant gain, especially if compared with the 10-fold increase in the neutron flux at the new Spallation Neutron Source in the United States compared with a much older similar facility, ISIS, in the United Kingdom. In addition to the gain in the signal rate, the mirror-based instrument could reach lower momentum transfer than most of the existing facilities¹⁰. To demonstrate this novel concept, in this work we have built a prototype Wolter-mirror-based SANS instrument at Oak Ridge National Laboratory (ORNL). The performance of this instrument, as described below, is in accord with computer simulations and is comparable to that of conventional facilities, even though it is equipped with very small prototype optics. Much larger mirrors can be manufactured for high-performance future facilities. Our demonstration, together with the earlier ray-tracing analysis¹⁰, opens the way for changing SANS instruments from pinhole cameras into microscopes, bringing transformative improvements to rate-limited neutron methods and enabling new science.

Results

Experimental setup. We tested the prototype SANS instrument at an instrument development beamline at ORNL¹⁴. A schematic layout of the experimental setup is shown in Fig. 1. The mirrors have the role of lenses, creating an image of the source aperture at the detector¹³. The mirrors used in this experiment consist of sections of confocal ellipsoid and hyperboloid. Incident rays must reflect from inside surfaces of the optics (ellipsoid, followed by the hyperboloid) before coming to focus. The rays, which do not intersect the first mirror, are stopped by a beamstop in front of the mirrors. The optics used in this experiment is made of three nested co-axial confocal Ni mirrors to improve the throughput. The device, fabricated at NASA using an electroformed replication process, has been used in previous demonstrations of neutron focusing and a neutron microscope^{13, 15}. For additional drawings and photographs of the setup, see Supplementary Figs S1–S3.

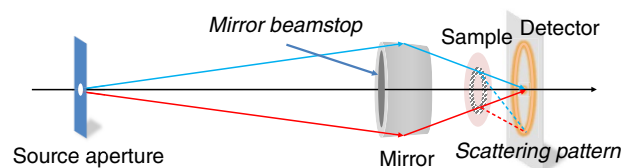


Figure 1 | Schematic layout of the focusing-mirror-based SANS

instrument. The source aperture and the detector are located at two foci of the mirror. A sample is placed between the optics and the detector. Solid lines indicate trajectories of incident and reflected neutrons, focused at the detector. Dashed lines indicate trajectories of neutrons scattered by the sample. The shaded area of the sample indicates the area, which is illuminated by the beam. The drawing of the mirror is not to scale, as the length of the optics is only 60 mm and the distance from the source to the detector is 3.2 m. See Supplementary Figs S1–S3 for additional drawings and pictures of the optics and the setup.

The source aperture and the detector were at two foci of the optics (2.56 m upstream and 0.64 m downstream, respectively). Test samples were placed 0.08 m in front of the detector. The measurements were made in the time-of-flight (TOF) mode, using a neutron chopper installed 0.3 m upstream of the source aperture. The chopper has an opening of 2 degrees and a frequency of 40 Hz. The detector, a 50-mm-diameter micro-channel plate with 48- μm pixels, was triggered by the chopper and the position and the TOF of each detected neutron were recorded. First, the focal spot and the spectrum of reflected neutrons were measured without the sample. Neutrons from the moderator obey the Maxwell–Boltzmann distribution, which peaks at ~ 4 Å. The spectrum of the neutrons illuminating the sample is modified by the reflectivity of the mirrors. The spectrum measured at the detector starts from 5 Å and peaks at about 6.5 Å, in accord with expectations from ray tracing.

Small-angle scattering by test samples. Two standard test samples, porous silica (Porasil B) and silver behenate powder, were used to calibrate neutron intensity and the momentum transfer Q to measure the instrumental resolution and evaluate the low- Q limit of the prototype SANS.

Figure 2a displays experimental results for Porasil B, which is typically used for intensity calibrations of SANS instruments¹⁶. The scattering intensity from random interfaces in Porasil B is modelled by the Debye–Bueche formula: $I(Q) = I(0)(1 + \alpha^2 Q^2)^{-2}$, where the correlation length is $\alpha = 43.5 \pm 2$ Å. Figure 3b shows the Debye–Bueche plot ($I^{-1/2}$ versus Q^2) of the data. The linear fit in the range $0.0004 \text{ Å}^{-2} < Q^2 < 0.0012 \text{ Å}^{-2}$ gives $\alpha = 38 \pm 4$ Å, consistent with the nominal value. The plot shows that our prototype SANS instrument performs well at Q 's down to about 0.02 Å^{-1} .

The instrumental resolution is measured utilizing silver behenate, an organic compound, which has ordered lamellar structure. Its first Bragg peak at $Q_0 = 0.1076 \text{ Å}^{-1}$ is commonly used to calibrate momentum-transfer measurements¹⁷. The measured scattering pattern of silver behenate is shown in Fig. 3a, where the bright ring is because of the Bragg peak. The figure shows only neutrons from a narrow TOF band, corresponding to the wavelength $\lambda = 6.64 \text{ Å} \pm 2\%$. Figure 3b shows the same peak integrated over polar angles and wavelengths in the range from 6.4 to 9.2 Å. The width of the Bragg peak gives the Q resolution of the instrument: $\Delta Q/Q_0 \approx 14\%$, where ΔQ is the full-width at half-maximum (FWHM) of the Gaussian peak.

The momentum transfer at small angles $Q = (4\pi/\lambda) \sin(\theta/2) \cong 2\pi\theta/\lambda$ leads to the resolution $\Delta Q/Q_0 = \lambda^{-1} \Delta\theta(\lambda) 2\pi/Q_0$. $\Delta\theta(\lambda)$ is extracted

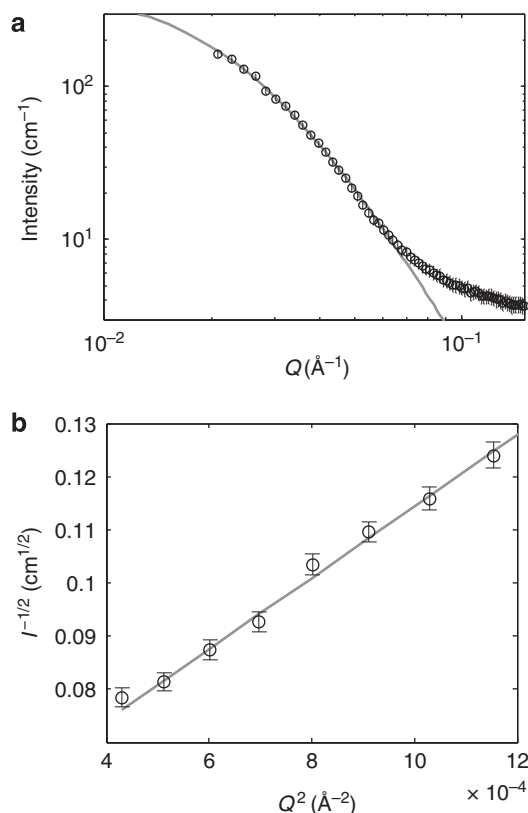


Figure 2 | SANS spectra from Porasil B. (a) The measured SANS curve. Error bars represent standard deviations derived from neutron counts. At low Q 's, the error bars are about the size of symbols. (b) The Debye-Bueche (D-B) plot of the same data. The D-B plot of the experimental data is linear down to $Q \sim 0.02 \text{ Å}^{-1}$. The dark grey lines (both in **a** and **b**) are the D-B model fit of the data.

at different wavelengths from the TOF measurements. The instrumental resolution as a function of the inverse neutron wavelength, $\Delta Q/Q_0(\lambda^{-1})$, is plotted in Fig. 4. This plot demonstrates that the resolution is determined by the size of the direct beam on the detector. Indeed, the direct beam is the demagnified image of the source aperture, which is 4 mm in diameter. The direct beam at the detector has a Gaussian profile with the FWHM about 1.25 mm, whereas the sample-to-detector distance (SDD) ≈ 80 mm, leading to $\Delta\theta \approx 0.016$ and $\Delta Q/Q_0 \approx 0.9\lambda^{-1}$, which coincides with the linear fit of the data in Fig. 4. Other contributions to the resolution, although insignificant, are discussed below.

Analysis of the instrument resolution. The resolution function of SANS instruments has contributions from uncertainties of neutron wavelengths and scattering angles^{18–20}. Therefore, the resolution is determined by the propagation of relative standard deviations $(\sigma_Q/Q)^2 = (\sigma_\lambda/\lambda)^2 + (\sigma_\theta/\theta)^2$. Here σ_Q , σ_λ and σ_θ denote standard deviations of the momentum transfer (Q), wavelength (λ) and scattering angle (θ), respectively. The beam at the source aperture has an approximate Gaussian profile. As the samples, the scattering cross-section, and the optics are axisymmetric, we use a one-dimensional approximation. In this case, the resolution $\Delta Q/Q \approx 2.35 \sigma_Q/Q$. Figure 5a shows the Q dependences of major contributions to the resolution function.

The uncertainty in the wavelength σ_λ is because of the finite opening in the beam chopper. The TOF is recorded for each

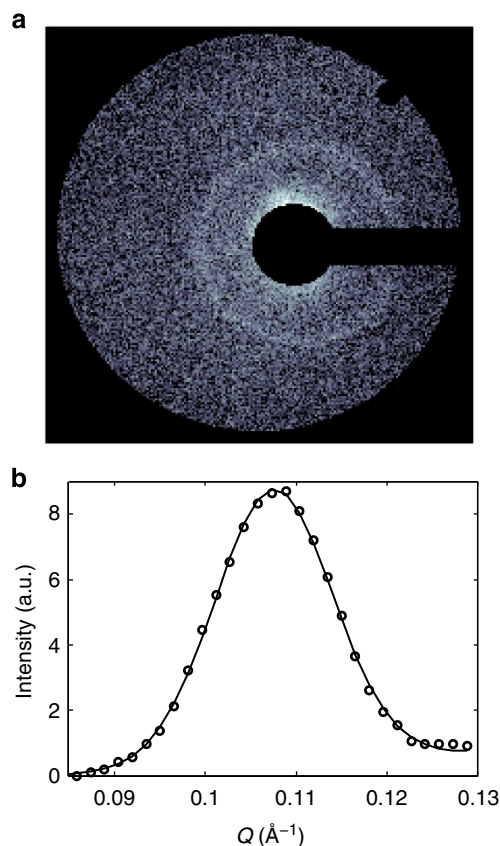


Figure 3 | Neutron diffraction from silver behenate. (a) Raw detector image, using monochromatic neutrons of $6.64 \text{ Å} \pm 2\%$ wavelength (corresponding to the time of flight of $5.88 \text{ ms} \pm 2\%$). The black area in the centre of the image masks the direct beam. The resolution of the detector is $1,024 \times 1,024$ with a $48\text{-}\mu\text{m}$ pitch. The bright ring is the diffraction peak at $Q_0 = 0.1078 \text{ Å}^{-1}$. (b) The diffraction peak after integration over the polar angle and wavelengths between 6.4 and 9.2 Å (open symbols). The solid line is a Gaussian fit. The FWHM of the peak (ΔQ) is 0.015 Å^{-1} , corresponding to the resolution ($\Delta Q/Q_0$) of about 14%.

neutron between the chopper and the detector and is used to calculate the wavelength: $\lambda(\text{Å}) = 3.956 \frac{\text{TOF}(\text{ms})}{L(\text{m})}$, where $L = 3.5$ m is the chopper-to-detector distance. Hence, $(\sigma_\lambda/\lambda)^2 = (\sigma_{\text{TOF}}/\text{TOF})^2$. The uncertainty of the TOF is because of the width of the chopper opening, which is 2 degrees in this experiment. At 40 Hz rotation frequency, the standard deviation of TOF is 0.04 ms by assuming uniform and constant beam flux. For the wavelength range of this experiment, $6.4\text{--}9.2 \text{ Å}$, corresponding TOF is from 5.67 to 8.14 ms, the standard deviation of 0.04 ms being $< 1\%$. As σ_λ has no momentum-transfer dependence, it is the horizontal line in Fig. 5a.

The uncertainty in the scattering angle has four contributions. In addition to the direct beam size (σ_b), other contributions include the detector pixel size (σ_p), figure errors of the mirrors (σ_{FE}) and the sample size (σ_d) (σ 's are variances of the position distributions of scattered neutrons on the detector). To summarize: $\sigma_\theta^2 = \frac{1}{\text{SDD}^2} (\sigma_b^2 + \sigma_p^2 + \sigma_{\text{FE}}^2 + \sigma_d^2)$. The direct beam on the detector is approximately Gaussian with the FWHM of 1.25 mm, leading to $1.25 \text{ mm} \approx 2.35 \sigma_b$. Therefore, the standard deviation of the angular resolution $\frac{\sigma_\theta}{\text{SDD}} \approx 6.65 \times 10^{-3}$. This is the largest contribution to the resolution function, decreasing with Q , as shown in Fig. 5a. The uncertainty because of the pixel size, $48 \mu\text{m}$ in this experiment, is much smaller than the direct beam size. σ_{FE} is determined by the deviation of the mirrors from the

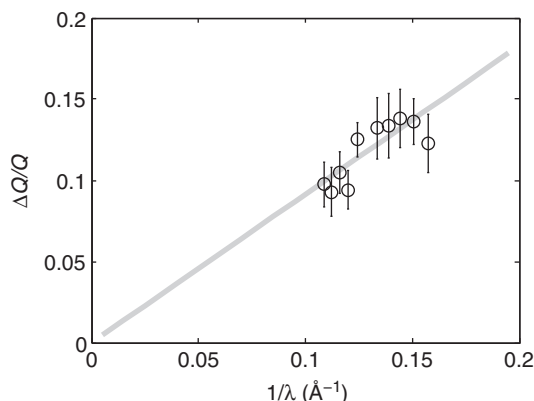


Figure 4 | Instrumental resolution as a function of the inverse neutron wavelength. Open symbols represent $\Delta Q/Q$, where $Q = 0.1078 \text{ \AA}^{-1}$ is the positions of the first diffraction peak of silver behenate, and ΔQ is the FWHM of the peak (see Fig. 3b), calculated from the Gaussian fit. Error bars represent 90% confidence interval. The grey line is the resolution function because of the size of the direct beam only (corresponding to σ_b in the text). It coincides with the linear fit of the data.

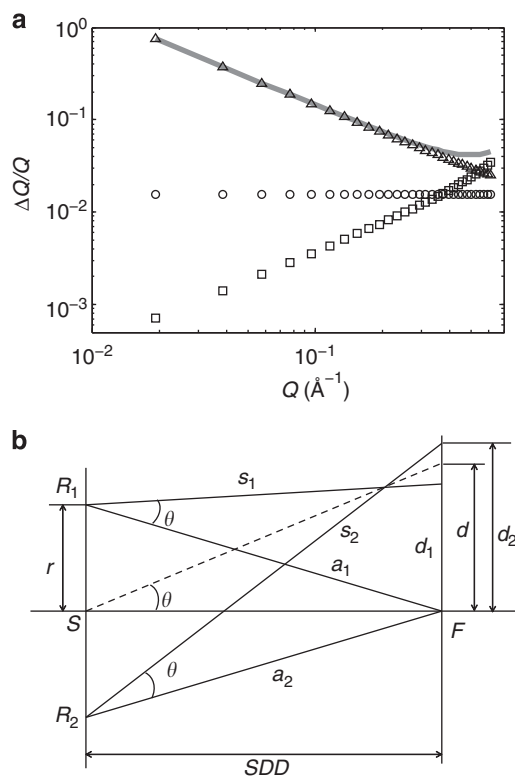


Figure 5 | Calculation of the instrumental resolution. (a) Components of the instrument resolution as a function of the wavenumber transfer. Squares, circles and triangles represent uncertainties because of the sample size, wavelength spread and the direct beam size, respectively. The thick grey line shows the overall effect. All the results are calculated at $\lambda = 6.8 \text{ \AA}$. (b) The geometry used to calculate the error of Q introduced by the sample size. S and F indicate the sample position (S is the centre of the sample ring) and the detector position (F is the focus). Neutrons reflected from axisymmetric optics form a thin ring of radius r . For simplicity, the thickness of the ring is not taken into account. θ is the scattering angle. Lines a_1 and a_2 are trajectories of the scattered neutrons from points R_1 and R_2 , which are located at the opposite sides of the ring. Line s_1 and s_2 are the trajectories of scattered neutrons.

ideal shape. The angular resolution of these mirrors is about $100 \mu\text{rad}$, corresponding to the positional uncertainty of $< 100 \mu\text{m}$ at the detector¹⁵, again much smaller than the direct beam size. Final contribution to the angular uncertainty, σ_d , is peculiar to the axisymmetric focusing optics. It arises because the sample behind the optics is illuminated by the ring of reflected neutrons. In this experiment, the ring diameter at the sample position was about 4 mm, whereas the SDD was about 80 mm. Figure 5b illustrates the geometry and notations. It shows two neutrons scattered with the same angle θ , but at diametrically opposite points on the ring, reaching the detector at different radii, d_1 and d_2 . Therefore, neutrons with the same scattering angle form a ring with the thickness $\delta d = |d_1 - d_2| = |\sqrt{a^2 + s_1^2 - 2as_1 \cos \theta} - \sqrt{a^2 + s_2^2 - 2as_2 \cos \theta}|$, where $a = a_1 = a_2$. Assuming that neutrons are uniformly distributed across δd , the standard deviation of positions across the scattering ring is $\sigma_d = \delta d / \sqrt{12}$. Numerical calculations of this effect show that it needs to be considered when $Q > 0.3 \text{ \AA}^{-1}$ for the particular geometry of this test (see Fig. 5b). In future focusing SANS instruments, the SDD will likely be much $> 80 \text{ mm}$, and therefore the effect of the ring size will be negligible even at large Q 's.

Discussion

Let us consider the performance of this prototype SANS instrument, especially at low- Q and high- Q regions, in the interest of future focusing-mirror-based SANS facilities.

The low- Q limit is determined by the size of the direct beam. For this experiment, we used the beamstop made of a 5-mm wide block of borated aluminium. It is actually larger than the footprint of the transmitted neutron on the detector (about 1.25 mm in diameter). In principle, when an ideal beamstop is installed, the minimum Q of this prototype can reach about $6.7 \times 10^{-3} \text{ \AA}^{-1}$ in our experimental configuration. It is at the same level as state-of-the-art conventional SANS instruments. If necessary, the low- Q limit can be further extended by using smaller source aperture or by installing another focusing mirror of smaller demagnification number.

The high- Q limit is determined by the detector's size. For example, if our prototype was equipped with a 100-mm-diameter detector, the highest Q value can reach about 1 \AA^{-1} beyond the required highest Q values for most SANS experiments. Figure 5a shows that the resolution at 1 \AA^{-1} will be about 10%, which is still very good for most SANS studies.

An important concern of SANS facilities is the background created by diffraction from mirror surface roughness. Such diffraction results in neutrons reflected at large angles (so-called off-specular reflections)²¹, potentially creating extra background for weak SANS signals, a limiting factor especially at high Q 's. We measured this background in our setup using the fact that off-specular scattering is strongly reduced below the cutoff wavelength corresponding to the critical angle. Therefore, we compared the background below and above the cutoff wavelength (about 5 \AA) and found no difference between these two cases. Hence, in our measurements, the background introduced by the mirrors is insignificant. Also note that the operating mirror-based SANS users' facility at FRM-II (Munich) does not suffer from effects of surface diffraction, thus demonstrating that state-of-the-art modern polishing techniques are good enough for this purpose²².

Gravity effects were not important for this demonstration experiment, as the mirror-to-mirror and SDDs were only 0.64 and 0.08 m correspondingly. Since most of the signal was due to neutrons of wavelengths around 6 \AA , the gravitational beam deflection was too small to cause a measurable effect. However, for longer future instruments, gravity should be analysed and

compensated, if needed, with the help of prisms—a standard method used at SANS facilities^{2,19,23}.

To discuss future practical implementations, let us refer to the optimized mirror, which is capable of increasing the signal rate of EQ-SANS—the SANS instrument at Spallation Neutron Source—by a factor of ≥ 50 , as described in Liu *et al.*¹⁰ The optic is an elliptical segment of 0.4 m length and 0.09 m radius. This is larger than the prototype device used here but manageable and entirely within the realm of the existing technology. (EQ-SANS is 13 m long. For shorter focal lengths, two-reflection mirrors should be utilized as in the ellipsoid–hyperboloid prototype used here.) We should note that the large signal rate increase results mostly from the increase in the solid angle of the beam, which illuminates the sample. Therefore, larger samples are necessary to maximize the gain in the signal rate at high resolution when samples are placed right behind the mirrors. Still, traditional pinhole SANS cannot take advantage of larger samples to increase the intensity, and smaller samples could be placed closer to the detector, leading to increased intensity at some expense to the resolution because of the shorter SDD. Also note that both the prototype and the mirror analysed in Liu *et al.*¹⁰ are made of only natural Ni. Supermirror Wolter optics is technologically possible²⁴ but is not necessary for SANS in most cases. Wolter optics for SANS could be designed and made within months for a fraction of a cost of a SANS instrument using standard ray tracing and proven technology. As such, it offers the potential of improving the performance of SANS facilities by orders of magnitude in terms of the signal rate, improve the resolution and make shorter instruments with simpler detectors.

References

- Guinier, A. & Fournet, G. In *Small-Angle Scattering of X-rays* (Wiley, 1955).
- Littrell, K. C. A comparison of different methods for improving flux and resolution on SANS instruments. *Nucl. Instr. Meth. A* **529**, 22–27 (2004).
- Kearney, P., Klein, A., Opat, G. & Gähler, R. Imaging and focusing of neutrons by a zone plate. *Nature* **287**, 313–314 (1980).
- Eskildsen, M. R. *et al.* Compound refractive optics for the imaging and focusing of low-energy neutrons. *Nature* **391**, 563–566 (1998).
- Choi, S. M., Barker, J., Glinka, C. J., Cheng, Y. T. & Gammel, P. L. Focusing cold neutrons with multiple biconcave lenses for small-angle neutron scattering. *J. Appl. Cryst.* **33**, 793–796 (2000).
- Oku, T. *et al.* A focusing-geometry small-angle neutron scattering instrument with a magnetic neutron lens. *J. Appl. Cryst.* **40**, s408–s413 (2007).
- Thiyagarajan, P. *et al.* The time-of-flight small-angle neutron diffractometer (SAD) at IPNS, Argonne National Laboratory. *J. Appl. Cryst.* **30**, 280–293 (1997).
- Grunzweig, C. *et al.* Multiple small angle neutron scattering: a new two-dimensional ultrasmall angle neutron scattering technique. *Appl. Phys. Lett.* **91**, 203504 (2007).
- Alefeld, B., Schwahn, D. & Springer, T. New developments of small angle neutron scattering instruments with focussing. *Nucl. Instrum. Methods Phys. Res. A* **274**, 210–216 (1989).
- Liu, D. *et al.* Axisymmetric Grazing-Incidence Focusing Optics for Small-Angle Neutron Scattering. *Nucl. Instrum. Methods Phys. Res. A* **686**, 145–150 (2012).
- Désert, S., Panzner, T. & Permingeat, P. Focusing neutrons with a combination of parabolic and elliptical supermirrors. *J. Appl. Cryst.* **46**, 35–42 (2013).
- Gubarev, M. V., Ramsey, B. D., Engelhaupt, D. E., Burgess, J. M. & Mildner, D. F. R. An evaluation of grazing-incidence optics for neutron imaging. *Nucl. Instrum. Methods Phys. Res. B* **265**, 626–630 (2007).
- Khaykovich, B., Gubarev, M., Bagdasarova, Y., Ramsey, B. & Moncton, D. From X-ray telescopes to neutron scattering: using axisymmetric mirrors to focus a neutron beam. *Nucl. Instrum. Methods Phys. Res. B* **631**, 98–105 (2011).
- Crow, L. *et al.* The CG1 instrument development test station at the high flux isotope reactor. *Nucl. Instr. Meth. A* **634**, S71–S74 (2011).
- Liu, D. *et al.* Demonstration of achromatic cold-neutron microscope utilizing axisymmetric focusing mirrors. *Appl. Phys. Lett.* **102**, 183508 (2013).
- Wignall, G. T. & Bates, F. Absolute calibration of small-angle neutron scattering data. *J. Appl. Crystallogr.* **20**, 28–40 (1987).
- Gilles, R., Keiderling, U. & Wiedenmann, A. Silver behenate powder as a possible low-angle calibration standard for small-angle neutron scattering. *J. Appl. Cryst.* **31**, 957–959 (1998).
- Mildner, D. T. & Carpenter, J. Optimization of the experimental resolution for small-angle scattering. *J. Appl. Cryst.* **17**, 249–256 (1984).
- Hammouda, B. & Mildner, D. F. Small-angle neutron scattering resolution with refractive optics. *J. Appl. Cryst.* **40**, 250–259 (2007).
- Zhao, J., Gao, C. & Liu, D. The extended Q-range small-angle neutron scattering diffractometer at the SNS. *J. Appl. Cryst.* **43**, 1068–1077 (2010).
- Sinha, S., Sirota, E., Garoff, S. & Stanley, H. X-ray and neutron scattering from rough surfaces. *Phys. Rev. B* **38**, 2297–2311 (1988).
- Goerigk, G. & Varga, Z. Comprehensive upgrade of the high-resolution small-angle neutron scattering instrument KWS-3 at FRM II. *J. Appl. Cryst.* **44**, 337–342 (2011).
- Forgan, E. & Cubitt, R. Cancellation of gravity for slow neutrons in small angle scattering experiments. *Neutron News* **9**, 25–31 (1998).
- Gubarev, M. V. *et al.* From x-ray telescopes to neutron focusing. *Proc. SPIE* **8147**, 81470B (2011).

Acknowledgements

We acknowledge useful discussions with Dr. D.F.R. Mildner (NIST). Research has been supported by the US Department of Energy, Office of Basic Energy Sciences, Division of Materials Sciences and Engineering under Awards no. DE-FG02-09ER46556 and no. DE-FG02-09ER46557. The work at ORNL has been sponsored by the Basic Energy Science (BES) Program, Office of Science, US Department of Energy under contract number DE-AC05-00OR22725 with UT-Battelle, LLC.

Author contributions

B.K., D.L. and M.V.G. designed the experiment; D.L., B.K., M.V.G., J.L.R. and L.C. conducted the experiment; D.L. and B.K. analysed the data; M.V.G. and B.D.R. made the mirrors; B.K., D.L. and D.E.M. wrote the manuscript; B.K. and D.E.M. supervised the project.

Additional information

Supplementary Information accompanies this paper at <http://www.nature.com/naturecommunications>

Competing financial interests: The authors declare no competing financial interests.

Reprints and permission information is available online at <http://npg.nature.com/reprintsandpermissions/>

How to cite this article: Liu, D. *et al.* Demonstration of a novel focusing small-angle neutron scattering instrument equipped with axisymmetric mirrors. *Nat. Commun.* 4:2556 doi: 10.1038/ncomms3556 (2013).